# Voxel-Based 3-D Modeling of Individual Trees for Estimating Leaf Area Density Using High-Resolution Portable Scanning Lidar

Fumiki Hosoi and Kenji Omasa

***Abstract*—A method for accurate estimation of leaf area density (LAD) and the cumulative leaf area index (LAI) profiles of small trees (*Camellia sasanqua* and *Deutzia crenata*) under different conditions was demonstrated, which used precise voxel-based tree models produced by high-resolution portable scanning lidar. In this voxel-based canopy profiling (VCP) method, data for each horizontal layer of the canopy of each tree were collected from symmetrical azimuthal measurement points around the tree using optimally inclined laser beams. The data were then converted into a voxel-based three-dimensional model that reproduced the tree precisely, including within the canopy. This precise voxel model allowed the LAD and LAI of these trees, which have extremely dense and nonrandomly distributed foliage, to be computed by direct counting of the beam-contact frequency in each layer using a point-quadrat method. Corrections for leaf inclination and nonphotosynthetic tissues reduced the estimation error. A beam incident zenith angle near 57.5° offered a good correction for leaf inclination without knowledge of the actual leaf inclination. Nonphotosynthetic tissues were removed by image-processing techniques. The best LAD estimations showed errors of 17% at the minimum horizontal layer thickness and of 0.7% at the maximum thickness. The error of the best LAI estimations was also 0.7%.**

***Index Terms*—Leaf area density (LAD), leaf area index (LAI), portable scanning lidar, tree, voxel-based model.**

## I. Introduction

THE FOREST canopy has the important functional roles of cycling material and energy through photosynthesis and transpiration, maintaining forest microclimates, and providing habitats for various species. Determining the vertical structure of the canopy is very important because the three-dimensional (3-D) composition of the canopy helps sustain these functional roles. The vertical foliage structure is often represented by the leaf area density (LAD) in each horizontal layer, where LAD is defined as the total one-sided leaf area per unit layer volume [1]. The leaf area index (LAI), which is defined as the leaf area per unit ground area, is calculated by integrating the LAD data.

The point-quadrat method was first developed as an indirect method of measuring LAD and LAI [2], [3]. In this method, a probe with a sharp point is inserted into the canopy at a known inclination and azimuth angle, and the number of times the point contacts leaves or stems is counted. LAD and LAI can then be estimated by calculating the contact frequency, which is defined as the mean number of contacts per insertion. The contact frequency is a useful quantity for estimating LAD and LAI, because no assumptions on leaf spatial distribution, shape, or size are required [1]. However, because this method requires many insertions of the probe into the actual canopy, it is very laborious [4].

Another indirect method, the gap-fraction method, is widely applied in field surveys, and it uses commercially available tools such as a camera with a fish-eye lens or the LI-COR LAI-2000 Plant Canopy Analyzer [5], [6]. This method allows automatic estimation of LAI without destruction of the plants and is less laborious. However, it requires the assumption that the foliage distribution is random, which leads to underestimation of LAI when leaves are clumped or overlapping. Moreover, the estimate is accurate only for diffuse light filtered through the canopy; direct sunlight introduces error.

Recently, light detection and ranging (lidar), a 3-D remote-sensing technique, has been applied to forests. Lidar instruments mounted on aircraft—airborne lidar—can scan the forest canopy of an entire region by emitting and receiving laser pulses, and the results are not affected by varying light conditions [7]–[9]. Large-footprint airborne lidar has been used to estimate the vertical canopy surface profile on the basis of the waveforms of returned pulses [10], [11]. Although this system has been proven useful on regional scale, the image resolution and information on the inner part of the canopy that it provides are limited. In contrast, commercially available aircraft-mounted lidar instruments with fine spatial resolution can provide precise profiles of canopy height [12]–[15]. This type of lidar, however, receives basically only the first and last returned pulses, with the result that little information on the inner part of canopy is obtained [16].

A portable ground lidar system, however, can complement the weak points of airborne lidar in forest applications. Its fine spatial resolution and small beam size allow the inner canopies of trees to be measured from the ground, making an accurate estimation of LAD profiles possible. Portable lidar instruments have been used previously for forest-canopy observation [17]–[19]. Radtke and Bolstad [18] and Parker *et al.* [19] used a nonscanning lidar (range finder) to emit vertical laser pulses upward from the ground to estimate LAD by an optical point-quadrat method [20]. This method is a kind of

Manuscript received September 25, 2005; revised March 31, 2006.

The authors are with Graduate School of Agricultural and Life Sciences, The University of Tokyo, Tokyo 113-8657, Japan (e-mail: aomasa@mail.ecc.u-tokyo.ac.jp).

Digital Object Identifier 10.1109/TGRS.2006.881743

TABLE I
PARAMETERS OF EACH OF THE TWO TREE SPECIMENS, *C. sasanqua* AND *D. crenata*

| Tree | Height (m) | LAI ($m^2/m^2$) | [a]LAD ($m^2/m^3$) | | Leaf inclination angle (degree) | | Leaf size (mm) | | | | Stem diameter (mm) |
|---|---|---|---|---|---|---|---|---|---|---|---|
| | | | | | | | Length | | Width | | |
| | | | Mean | Max | Mean | S.D.[b] | Mean | S.D.[b] | Mean | S.D.[b] | |
| *Camellia sasanqua* | 1.60 | 6.5 | 4.4 | 7.3 | 19.5 | 15.3 | 44.8 | 4.7 | 20.2 | 2.5 | 33.3 |
| *Deutzia crenata* | 0.60 | 2.8 | 4.7 | 11.2 | 20.2 | 16.9 | 48.5 | 8.4 | 19.9 | 3.1 | 6.2 |

[a]LAD : The LADs of *Camellia sasanqua* and *Deutzia crenata* were estimated at horizontal layer thicknesses of 0.1 and 0.05m, respectively.
[b]S.D. = Standard deviation

gap-fraction method rather than a standard point-quadrat method, because LAD is estimated from the gap fractions observed in each horizontal layer. The LAD is thus often underestimated when the distribution of foliage is nonrandom [18], [21], so a calibration using measured LAI values is required to obtain absolute LAD values. In addition, when the foliage density is high, vertical laser-beam penetration of the horizontal layers is uneven because fewer laser beams reach the upper canopy. For example, Lovell *et al.* [16] reported obtaining better measurements from the ground for the lower canopy than the upper canopy with portable scanning lidar. Moreover, nonphotosynthetic tissues such as stem and branches are not distinguishable from leaves, and it was also difficult to correct for leaf-inclination angle by previous portable lidar methods. Finally, measuring the horizontal differences in the foliage is very labor intensive. Therefore, we developed a practical method for accurate LAD estimation using a high-resolution portable scanning lidar, which we refer to as the voxel-based canopy profiling (VCP) method.

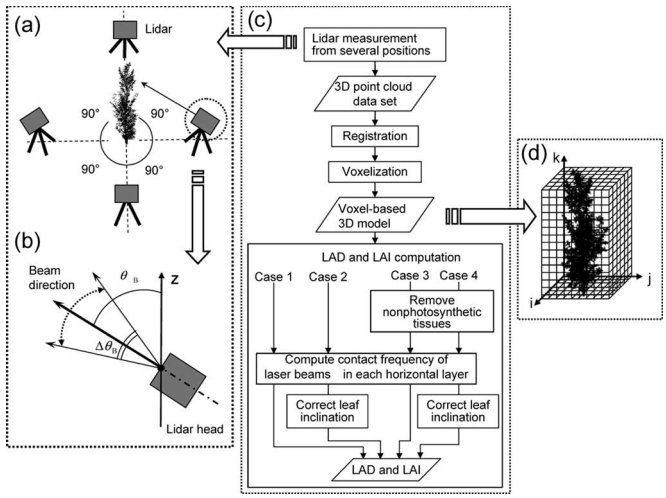


Fig. 1. Schematic diagram of the lidar-measurement technique for estimating LAD and LAI using a voxel-based 3-D tree model. (a) Positions used for lidar measurements around each tree. (b) Laser-beam inclination represented by the central zenith angle of the laser scan ($\theta_B$) and the zenith scan angle ($\Delta\theta_B$), (c) flow chart showing the steps of LAD and LAI computation, and (d) illustration of a voxel-based tree model.

## II. MATERIALS AND METHODS

### A. Plant Materials and Their Characteristics

We tested our method on two species of small tree: *Camellia sasanqua* and *Deutzia crenata* (Table I). The actual LAD values of each horizontal layer of *C. sasanqua* and *D. crenata* were measured by stratified clipping for layer thicknesses of 0.1 and 0.05 m, respectively. For this measurement, all leaves in each horizontal layer of *C. sasanqua* and *D. crenata* were clipped and scanned into JPEG images using a commercially available desktop scanner (FB636U, Canon, Inc.). The relationship between the number of pixels within the images and actual area (square meters) was determined by scanning a ruler together with the leaves. The number of pixels of leaves within the images was then converted into the actual leaf area of the leaves using the relationship. The actual LAD in each horizontal layer was obtained by dividing the actual area in each horizontal layer by the horizontal layer thickness and the area of the projection of the sample tree's canopy onto the ground. These values were then integrated with respect to height to obtain LAI. The LAI and LAD of the two specimens were similar or somewhat higher than those of forest stands. Therefore, the levels of LAI and LAD seemed to be suitable for confirming the validity and the robustness of our method.

### B. Measurement by Portable Scanning Lidar

A fine-resolution portable scanning lidar (TDS-130L 3-D laser scanner, Pulstec Industrial Co., Ltd) was used to measure each tree from several positions [Fig. 1(a)]. The range accuracy was about 2 mm, and the scan resolution was about 1 mm. A rotating mount run by a built-in stepping motor and a galvano mirror within the lidar head facilitated horizontal and vertical scanning by the instrument.

Different laser-beam inclinations and lidar positions were tested to obtain better information on the LAD profiles of each horizontal layer of the trees. Although the laser inclination, which is defined by both the central zenith angle of the laser scan $\theta_B$ and the zenith scan angle $\Delta\theta_B$ [Fig. 1(b)], greatly influences the accuracy of LAI and LAD estimation, at the beginning of the experiment, the optimal laser inclination was unknown. Therefore, the trees were scanned by using zenith scan angles from 8° to 14° at central zenith angles of 37.5°, 59.8°, 77.3°, and 180° for *C. sasanqua* and 16.2°, 55.7°, and 180° for *D. crenata* (a central zenith angle of 180° means that the laser beam was emitted from directly above the top of the tree) from four positions [Fig. 1(a) and (b)]. The horizontal scan angle was set at about 5° to cover the width of the materials.

Three-dimensional point cloud data for each central zenith angle and each position were recorded. The tree element positions in the 3-D point cloud data were represented as points in orthogonal coordinate systems. The measurements were first carried out for the intact, leaved trees, and then they were repeated for only nonphotosynthetic tissues, after removal of the leaves from the same trees.

### C. Generation of the Voxel-Based 3-D Tree Model

The voxel-based 3-D tree model was generated in several steps [Fig. 1(c), upper panel].

*1) Registration Process:* The complete data set for each central zenith angle was composed of four-point cloud data, one obtained from each of the four azimuthal positions. These four data with their individual coordinate systems were registered into a single-point cloud data set with a common coordinate system by using the iterative closest point algorithm [22].

*2) Voxelization:* A voxel-based tree model for each central zenith angle was produced from the registered point cloud data set. A voxel is defined as a volume element in a 3-D array. All points within the registered data set were converted into voxel coordinates by the following equations:

$$i = \mathrm{Int}\left(\frac{X - X_{\min}}{\Delta i}\right) \tag{1}$$

$$j = \mathrm{Int}\left(\frac{Y - Y_{\min}}{\Delta j}\right) \tag{2}$$

$$k = \mathrm{Int}\left(\frac{Z - Z_{\min}}{\Delta k}\right) \tag{3}$$

where $(i, j, k)$ are the voxel coordinates in the voxel array, Int is a function to round off at one decimal place to the nearest integer, $(X, Y, Z)$ represent the point coordinates of the registered lidar data, $(X_{\min}, Y_{\min}, Z_{\min})$ are the minimum values of $(X, Y, Z)$, and $(\Delta i, \Delta j, \Delta k)$ represent the voxel element size. In this experiment, the voxel element size, which depends on the range and scan resolution of the lidar, was $1 \times 1 \times 1$ mm; thus, the 3-D array was composed of $700 \times 700 \times 1600$ voxels for *C. sasanqua* and $600 \times 600 \times 600$ voxels for *D. crenata* [see Fig. 1(d)]. Voxels corresponding to voxel coordinates converted for all points within the registered data set were assigned attribute 1. A voxel with attribute 1 represents a voxel, in which the laser beams were intercepted. Other attributes for the remaining voxels, in which the laser beams were not intercepted, are assigned in next section.

### D. LAD and LAI Computational Models

LAD and LAI were computed for four cases [Fig. 1(c), lower panel], with or without corrections for leaf inclination and nonphotosynthetic tissues (stem and branches), of the voxel-based tree model.

*1) Removal of Nonphotosynthetic Tissues:* For each species, two voxel-based tree models, one for the intact, leaved tree and the other for only nonphotosynthetic tissues, were obtained as described in Section II-C above, "Generation of the Voxel-Based 3-D Tree Model." The voxel-based tree model that excluded nonphotosynthetic tissues was obtained by subtracting the nonphotosynthetic tissue model from the leaved tree model.

*2) Computation of the Contact Frequency of the Laser Beams in Each Horizontal Layer:* For computation of LAD and LAI, a plant region is set in a voxel array. The plant region is defined as the region above an area covered by a projection of the canopy on the horizontal plane [see Fig. 3(a)]. The area covered by the projection of the canopy is produced in a voxel array by projecting all voxels with attribute 1 onto the horizontal plane at $k = 0$. Voxels above the area are regarded as voxels within the plant region, and they are used for LAD and LAI computation.

LAD between height $h$ and $h + \Delta H$ above the ground $\mathrm{LAD}(h, \Delta H)$ is given by

$$\mathrm{LAD}(h, \Delta H) = \frac{1}{\Delta H} \sum_{k=m_h}^{m_{h+\Delta H}} l(k) \tag{4}$$

where $l(k)$ is the LAI of the $k$th horizontal layer of the voxel array within a plant region, $\Delta H$ is the horizontal layer thickness, and $m_h$ and $m_{h+\Delta H}$ are the voxel coordinates on the vertical axis equivalent to height $h$ and $h + \Delta H$ in orthogonal coordinates $(h = \Delta k \times m_h)$. The LAI of the $k$th horizontal layer $l(k)$ is the product of the contact frequency $N(k)$ of laser beams in the $k$th layer and the coefficient $\alpha(\theta)$, which corrects for leaf inclination at laser incident zenith angle $\theta$

$$\begin{aligned} l(k) &= \alpha(\theta) N(k) \\ &= \alpha(\theta) \cdot \frac{n_{\mathrm{I}}(k)}{n_{\mathrm{I}}(k) + n_{\mathrm{P}}(k)} \end{aligned} \tag{5}$$

where $n_{\mathrm{I}}(k)$ is the number of laser beams intercepted by the $k$th layer, $n_{\mathrm{P}}(k)$ is the number of laser beams passed through the $k$th layer, and $n_{\mathrm{I}}(k) + n_{\mathrm{P}}(k)$ is the total number of incident laser beams that reach the $k$th layer. $\alpha(\theta)$ is expressed in terms of $G(\theta)$, which is the mean projection of a unit leaf area on a plane perpendicular to the direction of the laser beam [1], [4]–[6]

$$\alpha(\theta) = \frac{\cos\theta}{G(\theta)}. \tag{6}$$

$G(\theta)$ is determined with the assumption that leaves are positioned symmetrically with respect to the azimuth, as follows (see Fig. 2):

$$\begin{aligned} G(\theta) &= \frac{1}{2\pi} \int_0^{2\pi} \int_0^{\pi/2} g(\theta_{\mathrm{L}}) \left|\cos(\vec{n}_{\mathrm{B}}, \vec{n}_{\mathrm{L}})\right| d\theta_{\mathrm{L}} d\varphi_{\mathrm{L}} \\ &= \int_0^{\pi/2} g(\theta_{\mathrm{L}}) S(\theta, \theta_{\mathrm{L}}) d\theta_{\mathrm{L}} \end{aligned} \tag{7}$$

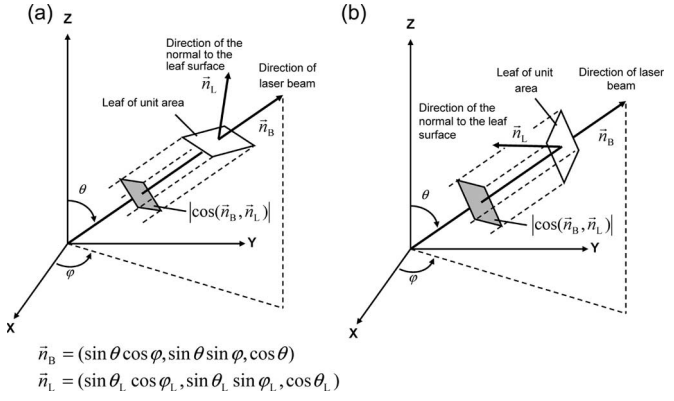


Fig. 2. Schematic diagram of the projection of a unit leaf area on a plane perpendicular to the direction of the laser beam. $\theta$ is the laser-beam incident zenith angle, and $\theta_{\rm L}$ is the leaf-inclination angle (the zenith angle of the normal to the leaf surface), and $\varphi$ and $\varphi_{\rm L}$ are the azimuth angles of the laser beam and the normal to the leaf surface, respectively. $\vec{n}_{\rm B}$ and $\vec{n}_{\rm L}$ are unit vectors corresponding to the direction of the laser beam and the direction of the normal to the leaf surface, respectively. $|\cos(\vec{n}_{\rm B}, \vec{n}_{\rm L})|$ is the absolute value of the cosine of the angle between $\vec{n}_{\rm B}$ and $\vec{n}_{\rm L}$, which is the projection of a unit leaf area on a plane perpendicular to the direction of the laser beam $\vec{n}_{\rm B}$: (A) $\theta \leq \pi/2 - \theta_{\rm L}$ and (B) $\theta > \pi/2 - \theta_{\rm L}$.

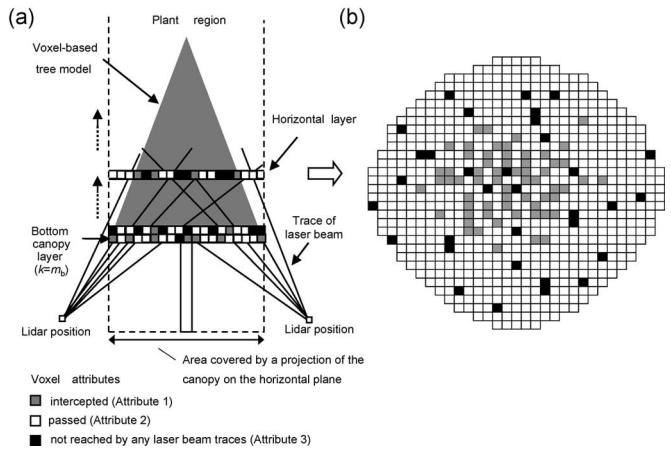


Fig. 3. Schematic diagram of the laser beam tracing process in the voxel array. (a) Laser beam tracing for determining voxel attributes (1, intercepted; 2, passed; and 3, not reached by any laser beam traces). The plant region is defined as the region above an area covered by a projection of the canopy on the horizontal plane (between the broken lines). The bottom canopy layer is the lowest horizontal layer that includes voxels corresponding to leaves. (b) Example of attribute assignment to voxels within a horizontal layer.

where

$$S(\theta,\theta_{\rm L}) = \frac{1}{2\pi}\int_0^{2\pi} |\cos(\vec{n}_{\rm B},\vec{n}_{\rm L})|\, d\varphi_{\rm L}$$

$$= \frac{1}{2\pi}\int_0^{2\pi} |\cos\theta\cos\theta_{\rm L} + \sin\theta\sin\theta_{\rm L}\cos(\varphi-\varphi_{\rm L})|\, d\varphi_{\rm L}$$

$$= \begin{cases} \cos\theta\cos\theta_{\rm L}, & \text{for } \theta \leq \frac{\pi}{2} - \theta_{\rm L} \\ \cos\theta\cos\theta_{\rm L}\left[1 + \frac{2(\tan x - x)}{\pi}\right], & \text{for } \theta > \frac{\pi}{2} - \theta_{\rm L} \end{cases} \tag{8}$$

$$x = \cos^{-1}(\cot\theta\cot\theta_{\rm L}). \tag{9}$$

$\theta_{\rm L}$ is the leaf-inclination angle (the zenith angle of the normal to the leaf surface), and $\varphi$ and $\varphi_{\rm L}$ are the azimuth angles of the laser beam and the normal to the leaf surface, respectively. $g(\theta_{\rm L})$ is the distribution function of the leaf-inclination angle; it is independent of the azimuth angle of the normal to the leaf surface, assuming azimuth symmetry. $|\cos(\vec{n}_{\rm B}, \vec{n}_{\rm L})|$ is the absolute value of the cosine of the angle between two unit vectors corresponding to the direction of the laser beam and the direction of the normal to the leaf surface. This value is the projection of a unit leaf area on a plane perpendicular to the direction of the laser beam $\vec{n}_{\rm B}$. $S(\theta,\theta_{\rm L})$ is the average of $|\cos(\vec{n}_{\rm B}, \vec{n}_{\rm L})|$ with respect to the azimuth angle of the normal to the leaf surface [2]. To use the actual measured distribution of leaf-inclination angles, (7) can also be expressed as follows:

$$G(\theta) = \sum_{q=1}^{T_q} g(q) S\left(\theta, \theta_{\rm L}(q)\right) \tag{10}$$

where $q$ is the leaf-inclination-angle class and $T_q$ is the total number of leaf-inclination-angle classes. Thus, if there are 18 leaf-inclination-angle classes from $0^\circ$ to $90^\circ$ ($T_q = 18$), then each class consists of a $5^\circ$ interval. For example, $q = 1$, $q = 9$, and $q = 16$ include the angles from $0^\circ$ to $4^\circ$, $40^\circ$ to $44^\circ$, and $75^\circ$ to $79^\circ$, respectively. $g(q)$ is the distribution of the leaf-inclination-angle class $q$, which is a ratio of the leaf area belonging to class $q$ to total leaf area; $\theta_{\rm L}({\rm q})$ is the midpoint angle of class $q$, which is the leaf-inclination angle used to represent class $q$. From (4) and (5), the LAD of each horizontal layer is expressed in terms of the product of the contact frequency sum and the correction coefficient $\alpha(\theta)$, on the assumption that $\alpha(\theta)$ is independent of the height $h$

$$\mathrm{LAD}(h,\Delta H) = \alpha(\theta)\cdot\frac{1}{\Delta H}\sum_{k=m_h}^{m_{h+\Delta H}} \frac{n_{\rm I}(k)}{n_{\rm I}(k)+n_{\rm P}(k)}. \tag{11}$$

Voxels that intercepted the laser beams have already been assigned attribute 1 in the voxelization process (see Section II-C). Therefore, $n_{\rm I}(k)$ is obtained by counting the number of voxels with attribute 1 in the $k$th layer of the voxel-based tree model. To obtain $n_{\rm P}(k)$, laser beams are traced in the tree model (see Fig. 3). The procedure starts from the bottom canopy layer within a plant region, which is the lowest horizontal layer, in which laser beams were intercepted by leaves (the vertical axis $k$ is represented as $m_{\rm b}$ at the bottom canopy layer). First, all laser beams emitted from all lidar positions are traced in the voxel array up to $k = m_{\rm b}$ in accordance with the actual lidar settings of the laser-beam angles. Next, voxels that do not have attribute 1 in the bottom canopy layer are considered. If one of the voxels is intersected by at least one laser-beam trace, the voxel is assigned attribute 2. A voxel with attribute 2 therefore represents a voxel through which a laser beam (or laser beams) passes. If a voxel that does not have attribute 1 in the bottom canopy layer is not intersected by any laser-beam traces, the voxel is assigned attribute 3. A voxel with attribute 3 represents a voxel that no laser beams can touch. By these procedures, all voxels that do not have attribute 1 in the bottom canopy layer are assigned attribute 2 or 3. Third,

traces of laser beams that intersect voxels with attribute 1 in the bottom canopy layer are not followed above that layer, because beams that have been intercepted in the bottom layer cannot reach any layers higher than the bottom canopy layer. Fourth, the remaining traces, that is, those beams not intercepted in the bottom canopy layer, are followed up to $k = m_{\rm b} + 1$ to determine the voxel attributes of the layer at $k = m_{\rm b} + 1$. In that layer, the procedures used to determine the voxel attributes of the bottom canopy layer are repeated using the traces still being followed. Similarly, traces that are not intercepted in the layer at $k = m_{\rm b} + 1$ are followed up to $k = m_{\rm b} + 2$, and the procedures used in the bottom canopy layer to determine voxel attributes are also repeated in the layer at $k = m_{\rm b} + 2$. The same procedures are repeated sequentially, layer by layer, up to the layer that corresponds to the tree top until finally the attributes of all voxels up to canopy top have been determined. Thus, $n_{\rm P}(k)$ is obtained by counting the number of voxels with attribute 2 in the $k$th layer.

The cumulative LAI from height $h$ to the height of the tree top HT can also be used to characterize the vertical profile of the foliage [18]. The cumulative LAI CLAI($h$) is given by the sum of contact frequency for $k = m_h$ to $k = m_{\rm HT}$ in (12), instead of $h$ to HT in height

$$\begin{aligned} {\rm CLAI}(h) &= \sum_{k=m_h}^{m_{\rm HT}} l(k) \\ &= \alpha(\theta) \cdot \sum_{k=m_h}^{m_{\rm HT}} \frac{n_{\rm I}(k)}{n_{\rm I}(k) + n_{\rm P}(k)} \end{aligned} \tag{12}$$

when $h$ is 0 (ground level), CLAI($h$) represents the LAI of the entire tree.

*3) Correction for Leaf Inclination:* Leaf inclination is corrected for by determining $\alpha(\theta)$ as in (6). The distribution of leaf inclination $g(q)$ is required to determine $\alpha(\theta)$ using (6), (8)–(10). $g(q)$ can be obtained by measuring the actual leaf-inclination angle of each leaf directly, but this is a laborious task. However, when the laser incident zenith angle $\theta$ is 57.5°, $\alpha(\theta)$ can be considered to be almost independent of leaf inclination: $\alpha(\theta) \cong 1.1$ [1], [3]. In this case, leaf inclination is well corrected for without any actual leaf-inclination data by using the following equation:

$${\rm LAD}(h, \Delta H) \cong 1.1 \times \frac{1}{\Delta H} \sum_{k=m_h}^{m_{h+\Delta H}} \frac{n_{\rm I}(k)}{n_{\rm I}(k) + n_{\rm P}(k)}. \tag{13}$$

From (12), CLAI($h$) for the particular case of $\theta = 57.5°$ is given by

$${\rm CLAI}(h) \cong 1.1 \times \sum_{k=m_h}^{m_{\rm HT}} \frac{n_{\rm I}(k)}{n_{\rm I}(k) + n_{\rm P}(k)}. \tag{14}$$

### E. Analysis of Measured Results

*1) Determination of the Optimal Laser Inclination:* From the voxel-based tree models excluding the nonphotosynthetic tissues, LAD profiles for different laser inclinations were computed by (11), with $\alpha(\theta)$ calculated by (6) and (8)–(10) from the leaf-inclination data obtained by actual measurement. The optimal conditions of laser inclination for the two specimens were determined by comparing the mean absolute percent errors (MAPE) between the calculated LAD profile and that obtained by stratified clipping.

*2) Error Analysis of LAD and LAI Computations:* The LAD profiles computed using the optimal laser inclination were compared among the four correction processes [cases 1 to 4, Fig. 1(c)]. Cumulative LAI profiles were also estimated and compared among the correction processes. The LAD and cumulative LAI profiles for cases 1 and 3, in which leaf inclination was disregarded, were computed by (11) and (12) with $\alpha(\theta) = 1$. Those for cases 2 and 4 were computed with the appropriate measurement-based values of $\alpha(\theta)$. For optimal laser inclinations close to 57.5°, LAD profiles were estimated by (13) and cumulative LAI profiles by (14).

To estimate the net errors of the LAD values for each correction process, the following equations were defined:

$$\begin{aligned} {\rm Error(case\ 1)} = {} & |{\rm MPE(case\ 1)} - {\rm MPE(case\ 3)}| \\ & + {\rm MAPE(case\ 3)} \end{aligned} \tag{15}$$

$$\begin{aligned} {\rm Error(case\ 2)} = {} & |{\rm MPE(case\ 2)} - {\rm MPE(case\ 4)}| \\ & + {\rm MAPE(case\ 4)} \end{aligned} \tag{16}$$

$${\rm Error(case\ 3)} = {\rm MAPE(case\ 3)} \tag{17}$$

$${\rm Error(case\ 4)} = {\rm MAPE(case\ 4)} \tag{18}$$

where MPE and MAPE are the mean percent error and the mean absolute percent error, respectively, for each correction process. Nonphotosynthetic tissues caused LAD to be overestimated, and leaf inclination caused LAD to be underestimated, so these errors tend to cancel each other out if they are not evaluated independently. Therefore, in cases 1 and 2, in which nonphotosynthetic tissues were not removed, the error caused by nonphotosynthetic tissues was separated for the net-error estimation by the expressions $|{\rm MPE(case\ 1)} - {\rm MPE(case\ 3)}|$ or $|{\rm MPE(case\ 2)} - {\rm MPE(case\ 4)}|$, as in (15) and (16).

Another possible cause of error are the differences in the vertical positions of the boundaries between the horizontal layers between the voxel-based tree model and the actual measurements, the magnitude of which depends on the horizontal layer thickness $\Delta H$. Therefore, (15)–(18) were used to analyze the errors for different values of $\Delta H$.

## III. Results

The voxel-based 3-D model (that for *C. sasanqua* is shown in Fig. 4) succeeded in reproducing each tree three-dimensionally at the individual leaf scale, although some noise spots are visible on the leaf edges [Fig. 4(c)].

To determine the optimal laser inclination, the LAD profiles of the voxel-based tree models that excluded the nonphotosynthetic tissues were compared among different laser inclinations. To calculate LAD using (11), $\alpha(\theta)$ was first computed with (6) and (8)–(10) from the actual measured leaf-inclination data. These procedures correspond to case 4 [Fig. 1(c)]. These

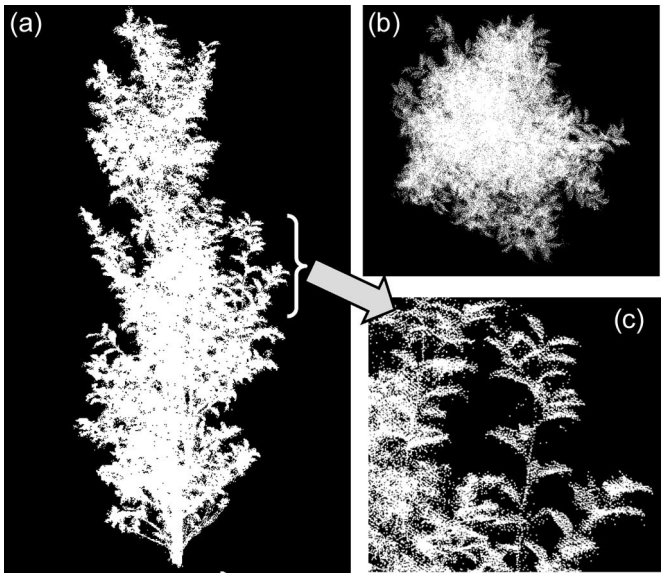


Fig. 4. Example of a voxelized *C. sasanqua* measured at $\theta_B = 59.8°$. Voxels with attribute of 1 are shown by white dots. (a) Side view, (b) top view, and (c) close-up view.

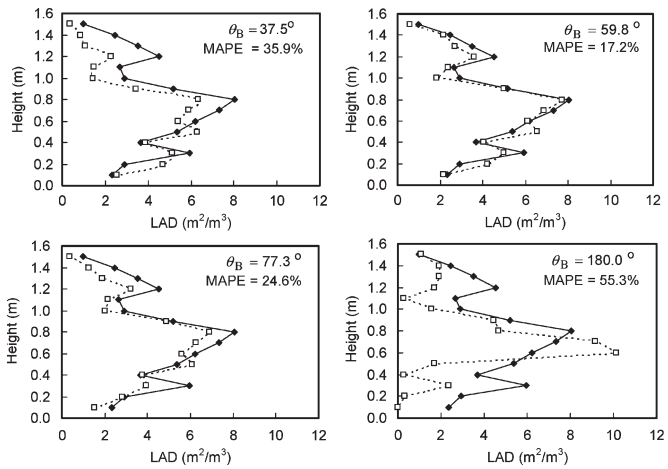


Fig. 5. Comparisons of LAD profiles for *C. sasanqua* between laser-derived estimates (white squares) obtained with different laser inclinations, $\theta_B$, and stratified-clipping values (black squares). MAPE—mean absolute percent error. $\Delta H = 0.1$ m. LAD was corrected for both leaf inclination and nonphotosynthetic tissues [case 4 in Fig. 1(c)].

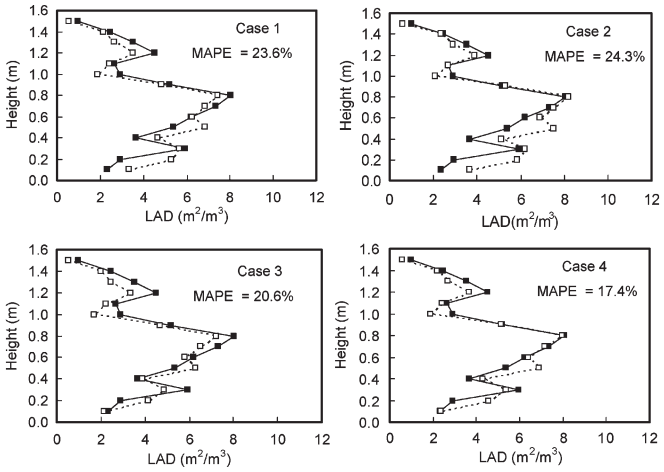


Fig. 6. Comparison of LAD profiles for *C. sasanqua* between laser-derived estimates (white squares) and stratified-clipping values (black squares) for each of the four correction process cases [Fig. 1(c)]. MAPE—mean absolute percent error. $\Delta H = 0.1$ m.

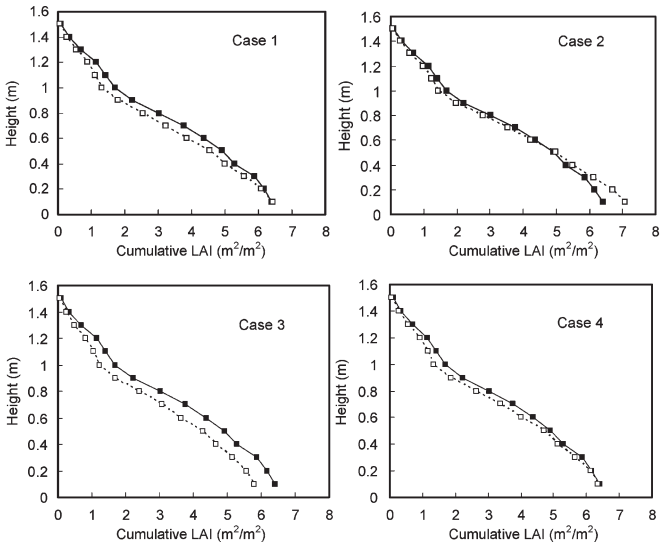


Fig. 7. Comparison of the cumulative LAI profiles for *C. sasanqua* between laser-derived estimates (white squares) and stratified-clipping values (black squares) for each of the four correction process cases [Fig. 1(c)]. $\Delta H = 0.1$ m.

laser-derived estimates were then compared with stratified-clipping values of the LAD profiles. The results for *C. sasanqua* at layer thickness $\Delta H = 0.1$ m are shown in Fig. 5. The error (MAPE) ranged from 17.2% to 55.3%. LAD was generally underestimated in the upper layer of the canopy for $\theta_B = 37.5°$, $59.8°$, and $77.3°$ and in both the upper and lower layers for $\theta_B = 180°$. The best central zenith angle $\theta_B$ for the laser scan was $59.8°$ for *C. sasanqua* and $55.7°$ for *D. crenata.* These angles are close to the particular angle $\theta_B = 57.5°$, described in Section II-D3 above, "Correction for Leaf Inclination," at which $\alpha(\theta)$ is almost independent of leaf inclination.

The laser-derived estimates produced by the procedures of cases 1–4 for *C. sasanqua* with $\theta_B = 59.8°$ were then compared with the stratified-clipping values of LAD profiles at $\Delta H = 0.1$ m (Fig. 6). Because $\theta_B$ was close to $57.5°$, (13), in which $\alpha(\theta) = 1.1$, was used to estimate LAD. The case 4 results fitted the actual LAD profiles best because both correction processes, removal of nonphotosynthetic tissues, and the correction for leaf inclination, were applied. The error (MAPE) was 17.4%, almost the same as that for $\theta_B = 59.8°$ with $\alpha(\theta)$ computed by (6) and (8)–(10) based on actual leaf inclination (Fig. 5). The case 1 results were also relatively accurate even though no correction processes were applied, because the error caused by nonphotosynthetic tissues was compensated for due to leaf inclination. The error in the case 2 results reflects nonphotosynthetic tissues, and that in the case 3 results is due to leaf inclination. LAD was generally underestimated in the upper part of the canopy and overestimated in the lower part. LAD was also computed by (13) for *D. crenata* because its optimum $\theta_B$ value was also near $57.5°$. As with *C. sasanqua*, the best result was obtained for case 4.

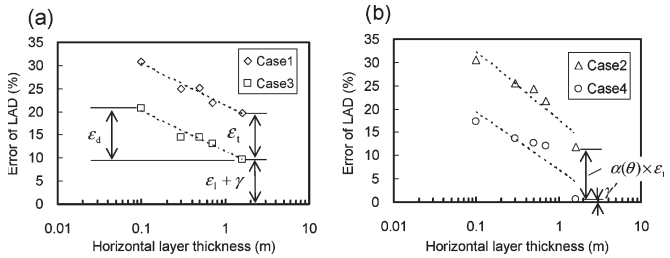


Fig. 8. Relationship between the horizontal layer thickness and LAD errors in each correction process for *C. sasanqua*: (a) No correction for leaf inclination and (b) correction of leaf inclination. See Fig. 1(c) for descriptions of cases. Errors were estimated by (15)–(18); $\varepsilon_t$, $\varepsilon_l$, and $\varepsilon_d$ represent the errors caused by nonphotosynthetic tissues, leaf inclination, and the layer boundary difference between the lidar measurement and stratified-clipping, respectively; $\gamma$ and $\gamma'$ represent the residual error in cases 3 and 4, respectively; and $\alpha(\theta)$ is the correction coefficient for leaf inclination.

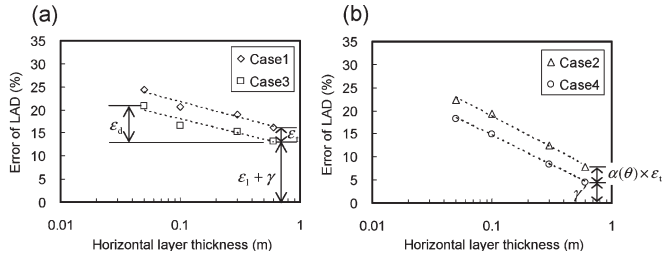


Fig. 9. Relationship between horizontal layer thickness and LAD errors in each correction process for *D. crenata*. (a) No correction for leaf inclination and (b) correction for leaf inclination. See Fig. 1(c) for descriptions of cases. Parameters are as in Fig. 8.

Fig. 7 shows cumulative LAI profiles of *C. sasanqua* for cases 1–4 at layer thickness $\Delta H = 0.1$ m. These profiles show the effects of the two correction processes more clearly, because variations in each horizontal layer are muted, making the general trend more apparent. In case 2, in which the correction for leaf inclination was applied but nonphotosynthetic tissues retained, the cumulative LAI was consequently overestimated at lower heights. In contrast, cumulative LAI in case 3 was underestimated because nonphotosynthetic tissues were removed but the leaf-inclination correction was not applied. In case 4, the match is excellent because both correction processes were applied. In case 1, the results are incidentally accurate because the errors caused by the presence of nonphotosynthetic tissues and by leaf inclination compensated for each other.

To clarify the independent effects of the two correction processes, the LAD errors in cases 1–4 were estimated by (15)–(18) and then compared with the horizontal layer thickness $\Delta H$ for *C. sasanqua* (Fig. 8) and for *D. crenata* (Fig. 9). In general, the larger the layer thickness became, the smaller the LAD error was in all cases. At the maximum layer thickness, that is, $\Delta H$ equal to the tree height (*C. sasanqua*, 1.6 m; *D. crenata*, 0.60 m), the tree was not divided into any horizontal layers; thus, the error caused by the difference in each horizontal layer boundary between the lidar measurement and stratified-clipping becomes zero.

For cases 1 and 3 of *C. sasanqua* [Fig. 8(a)], the error in the layer boundary difference $\varepsilon_d$ was 11% at $\Delta H = 0.1$ m compared with the error at $\Delta H = 1.6$ m. Cases 2 and 4 [Fig. 8(b)] were not suitable for estimating the net error of differences in the layer boundaries because of the bias caused by multiplication by the leaf-inclination correction coefficient $\alpha(\theta)$. In case 3 [Fig. 8(a)], the error caused by leaf inclination $\varepsilon_l$ and a residual error $\gamma$ remained at $\Delta H = 1.6$ m. The error caused by nonphotosynthetic tissues $\varepsilon_t$ was also present in case 1 [Fig. 8(a)] at $\Delta H = 1.6$ m. In contrast, the error at $\Delta H = 1.6$ m was less in case 2 [Fig. 8(b)] compared with that of case 1 [Fig. 8(a)], owing to the leaf-inclination correction. Moreover, only a slight residual error $\gamma'$ remained in case 4 [Fig. 8(b)] at $\Delta H = 1.6$ m, because both corrections had been applied. The error from the presence of nonphotosynthetic tissues $\varepsilon_t$ was estimated to be 10% by subtracting the case 3 error at $\Delta H = 1.6$ m from the corresponding case 1 error. The error due to leaf inclination $\varepsilon_l$ was similarly estimated to be 9% by subtracting the case 3 error at $\Delta H = 1.6$ m from the corresponding case 4 error. The final residual error $\gamma'$ in case 4 was 0.7%.

For *D. crenata*, in cases 1 and 3 [Fig. 9(a)], the error in the layer boundary difference $\varepsilon_d$ was 8% at $\Delta H = 0.05$ m. The error from nonphotosynthetic tissues $\varepsilon_t$ was estimated to be 3% by subtracting the case 3 error at $\Delta H = 0.60$ m from the corresponding case 1 error. $\varepsilon_t$ for *D. crenata* was smaller than that for *C. sasanqua*, because the stem diameter of the former was smaller than that of the latter (see Table I). The leaf-inclination error $\varepsilon_l$ was estimated to be 9% by subtracting the case 3 error at $\Delta H = 0.60$ m from the corresponding case 4 error. The final residual error $\gamma'$ in case 4 was 5%.

To summarize, the best LAD estimations for *C. sasanqua* were given in case 4, with an error of 17% at $\Delta H = 0.1$ m and of 0.7% at $\Delta H = 1.6$ m. Similarly, for *D. crenata*, case 4 resulted in the best estimations of LAD with an error of 18% at $\Delta H = 0.05$ m and of 5% at $\Delta H = 0.60$ m. The error in the layer boundary difference $\varepsilon_d$ might be improved by better alignment of the boundaries used in lidar measurement with those used for stratified clipping. The LAD error at maximum $\Delta H$ was the same as the overall LAI error for both species. Therefore, the errors of 0.7% in *C. sasanqua* and of 5% in *D. crenata* were also the best results in the overall LAI estimation.

## IV. Discussion

### A. Optimal Laser Inclination

The worst result was obtained for $\theta_B = 180°$ (Fig. 5). Although the lidar laser beams could illuminate the upper layer of the material at that inclination, for the most part, they could not reach the inner layers because the upper layer obstructed laser penetration. For $\theta_B = 37.5°$, LAD in the middle and upper layers was underestimated because the laser beams were obstructed by the lower layer. For $\theta_B = 77.3°$ and $59.8°$, the inclination of the laser beams resulted in less obstruction to laser penetration by the layers, so each layer was fully illuminated by the beams, thus yielding better results than the other two inclinations. Although the results for $\theta_B = 77.3°$ were comparable to those for the optimal inclination of $\theta_B = 59.8°$, at $\theta_B = 77.3°$, actual leaf-inclination data was required for the leaf-inclination correction. In contrast, because $\theta_B = 59.8°$ is nearly equal to the particular angle of 57.5° [1], [3], leaf

inclination can be well corrected for by setting $\alpha(\theta) = 1.1$ [see (13)] without requiring any actual leaf-inclination data. Thus, $\theta_{\mathrm{B}} = 59.8^{\circ}$ was not only optimal for beam penetration but also made this correction easier.

### B. Errors in LAD and LAI Estimation

LAD and cumulative LAI profiles for *C. sasanqua* in case 1 were apparently accurate, even though no correction process was applied (Figs. 6 and 7), because the effects of nonphotosynthetic tissues and leaf inclination canceled each other out. The error caused by nonphotosynthetic tissues was almost equal to that from leaf inclination (both errors were about 10%). These errors, however, should be separated for correct estimation of LAD and LAI.

The accuracy of LAD estimation, particularly at smaller values of $\Delta H$, was affected by the differences in layer boundaries between stratified clipping and lidar measurement. For the stratified clipping, the layer boundaries were measured using a ruler, and the scale was different from that used for the lidar measurement. The resulting slight differences in the vertical positions of the boundaries between the voxel-based model and the actual measurements led to an error that became larger at smaller $\Delta H$, when the layer boundary difference was not negligible relative to $\Delta H$. This error could be decreased by better alignment of the boundaries in the two measurement systems.

### C. Advantages of the Voxel-Based Technique

Conventional measurement by portable lidar results in uneven laser-beam penetration into each horizontal layer because penetration is less in the upper canopy [16]. In the present VCP method, each horizontal layer was scanned fully and evenly by optimally inclined laser beams emitted from several measuring points surrounding the specimen, thus solving the problem of unevenness of laser-beam penetration. Moreover, in the VCP method, full laser illumination within the canopy made it possible to count directly the contact frequency in each layer. The contact frequency is a useful quantity for estimating LAD and LAI, because no assumptions about leaf spatial distribution, shape, or size are required [1]. Therefore, underestimation caused by nonrandom foliage distribution, as reported previously [18], [21], can be avoided.

The voxel-based representation of the trees obtained by the VCP method has other advantages as well.

1) LAD and LAI computations are based not only on the points at which laser beams are intercepted, but also on those, through which the beams pass unobstructed. Because the information about each point is represented as a voxel with a particular attribution, voxel-based computation of LAD and LAI is easy.
2) The voxel-based 3-D array allows easy extraction of any sites required for computation by retrieving the voxel coordinates.
3) Overlapping points in the registered lidar data are represented as a single voxel; that is, the registered data are merged through the voxelization process. Therefore, overestimation of LAD caused by counting overlapping points is avoided through voxelization.
4) Voxelized lidar data can be treated as a 3-D image, so values can be computed by image-processing techniques. For example, nonphotosynthetic tissues were easily removed by subtracting the voxelized nonphotosynthetic tissues from the voxel-based tree model using image processing.

### D. Potential for Field Use and Other Applications

The significance of this VCP method is that LAD and LAI of trees can be estimated accurately without destruction of trees. This significance is greatly enhanced when the method is extended in field studies to larger trees. Optimally inclined laser beams with a zenith angle near 57.5° contributed to the better estimation of LAD in this paper. This particular angle also offered better estimation in previous field studies that used the gap-fraction method because of the insensitivity of that angle to leaf inclination [1], [23], [24]. Thus, this particular angle becomes a criterion for optimal beam inclination.

In the present technique, it is necessary to remove only nonphotosynthetic tissues from lidar data of leaved trees. Although the leaves were removed manually in this experiment, the natural defoliation of deciduous trees would permit easy data collection of only nonphotosynthetic tissues. Developing a method for removing nonphotosynthetic tissues using difference in reflectance of each part, i.e., leaf, branch, and trunk, of evergreen trees is a future challenge.

This precise voxel-based tree model is expected to be useful for obtaining other types of information about a tree. For example, Sinoquet and Rivet [25] computed branching pattern, fruit and shoot distribution, and plant topology using a precise 3-D model representing all vegetative components, which they constructed with an electromagnetic digitizer. Practical use of their method is limited, however, because a very large number of elements must be measured manually point by point. However, the present voxel-based model can easily provide estimates of various tree parameters by a 3-D image analysis.

The measurement range of our lidar system (less than 10 m) is insufficient for field application to large trees. However, a currently commercially available lidar system has a measurement range of up to several hundred meters, and this system could be used to test the validity of our method for large-tree measurements.

## V. Conclusion

The VCP method for accurate estimation of LAD and cumulative LAI profiles, which used precise voxel-based tree models produced by high-resolution portable scanning lidar, was demonstrated. Sufficient amounts of evenly distributed data on each horizontal layer throughout the canopy were collected by using optimally inclined laser beams and by taking measurements from symmetrical azimuthal measurement points. The data were converted into a voxel-based 3-D model that reproduced each tree precisely, including within the canopy. This precise voxel model made it possible to compute LAD and LAI by directly counting the contact frequency in each layer of the experimental trees.

In addition, corrections were applied for leaf inclination and the presence of nonphotosynthetic tissues, thus reducing the estimation error. A beam incident zenith angle near 57.5° made it possible to apply a good correction for leaf inclination without measuring the actual leaf inclination. By using a voxelized model, the nonphotosynthetic tissues were successfully removed by image-processing techniques. Therefore, it was possible to obtain good estimations of LAD and LAI with only small errors. This paper showed the fundamental method. The significance of the method is greatly enhanced when the method is applied in field studies to large trees, but further development is needed before it is ready for field application. We believe that additional work will enhance the validity of the method for various field applications.

## REFERENCES


[1] M. Weiss, F. Baret, G. J. Smith, I. Jonckheere, and P. Coppin, "Review of methods for *in situ* leaf area index (LAI) determination Part II. Estimation of LAI, errors and sampling," *Agric. For. Meteorol.*, vol. 121, no. 1/2, pp. 37–53, Jan. 2004.

[2] J. Warren-Wilson, "Inclined point quadrats," *New Phytol.*, vol. 59, no. 1, pp. 1–8, 1960.

[3] ——, "Estimation of foliage denseness and foliage angle by inclined point quadrats," *Aust. J. Bot.*, vol. 11, no. 1, pp. 95–105, 1963.

[4] I. Jonckheere, S. Fleck, K. Nackaerts, B. Muys, P. Coppin, M. Weiss, and F. Baret, "Review of methods for *in situ* leaf area index determination Part I. Theories, sensors and hemispherical photography," *Agric. For. Meteorol.*, vol. 121, no. 1/2, pp. 19–35, 2004.

[5] J. M. Norman and G. S. Campbell, "Canopy structure," in *Plant Physiological Ecology: Field Methods and Instrumentation*, R. W. Pearcy, J. Ehleringer, H. A. Mooney, and P. W. Rundel, Eds. London, U.K.: Chapman & Hall, 1989, pp. 301–326.

[6] J. M. Welles and J. M. Norman, "Instrument for indirect measurement of canopy architecture," *Agron. J.*, vol. 83, no. 5, pp. 818–825, 1991.

[7] M. Nilsson, "Estimation of tree heights and stand volume using an airborne lidar system," *Remote Sens. Environ.*, vol. 56, no. 1, pp. 1–7, Apr. 1996.

[8] E. Næsset, "Determination of mean tree height of forest stands using airborne laser scanner data," *ISPRS J. Photogramm.*, vol. 52, no. 2, pp. 49–56, Apr. 1997.

[9] J. E. Means, S. A. Acker, D. J. Harding, J. B. Blair, M. A. Lefsky, W. B. Cohen, M. E. Harmon, and W. A. McKee, "Use of large-footprint scanning airborne lidar to estimate forest stand characteristics in the Western Cascades of Oregon," *Remote Sens. Environ.*, vol. 67, no. 3, pp. 298–308, Mar. 1999.

[10] M. A. Lefsky, W. B. Cohen, G. G. Parker, and D. J. Harding, "Lidar remote sensing for ecosystem studies," *Bioscience*, vol. 52, no. 1, pp. 19–30, Jan. 2002.

[11] D. J. Harding, M. A. Lefsky, G. G. Parker, and J. B. Blair, "Laser altimeter canopy height profiles: Methods and validation for closed-canopy, broadleaf forests," *Remote Sens. Environ.*, vol. 76, no. 3, pp. 283–297, Jun. 2001.

[12] K. Omasa, Y. Akiyama, Y. Ishigami, and K. Yoshimi, "3-D remote sensing of woody canopy heights using a scanning helicopter-borne lidar system with high spatial resolution," *J. Remote Sens. Soc. Jpn.*, vol. 20, no. 4, pp. 394–406, 2000.

[13] K. Omasa, G. Y. Qiu, K. Watanuki, K. Yoshimi, and Y. Akiyama, "Accurate estimation of forest carbon stocks by 3-D remote sensing of individual trees," *Environ. Sci. Technol.*, vol. 37, no. 6, pp. 1198–1201, Mar. 2003.

[14] T. Brandtberg, T. A. Warner, R. E. Landenberger, and J. B. McGraw, "Detection and analysis of individual leaf-off tree crowns in small footprint, high sampling density lidar data from the eastern deciduous forest in North America," *Remote Sens. Environ.*, vol. 85, no. 3, pp. 290–303, 2003.

[15] M. Maltamo, K. Eerikäinen, J. Pitkänen, J. Hyyppä, and M. Vehmas, "Estimation of timber volume and stem density based on scanning laser altimetry and expected tree size distribution functions," *Remote Sens. Environ.*, vol. 90, no. 3, pp. 319–330, Apr. 2004.

[16] J. L. Lovell, D. L. B. Jupp, D. S. Culvenor, and N. C. Coops, "Using airborne and ground-based ranging lidar to measure canopy structure in Australian forests," *Can. J. Remote Sens.*, vol. 29, no. 5, pp. 607–622, 2003.

[17] K. Omasa, Y. Urano, H. Oguma, and Y. Fujinuma, "Mapping of tree position of Larix leptolepis woods and estimation of diameter at breast height (DBH) and biomass of the trees using range data measured by a portable scanning lidar," *J. Remote Sens. Soc. Jpn.*, vol. 22, no. 5, pp. 550–557, 2002.

[18] P. J. Radtke and P. V. Bolstad, "Laser point-quadrat sampling for estimating foliage-height profiles in broad-leaved forests," *Can. J. For. Res.*, vol. 31, no. 3, pp. 410–418, 2001.

[19] G. G. Parker, D. J. Harding, and M. L. Berger, "A portable LIDAR system for rapid determination of forest canopy structure," *J. Appl. Ecol.*, vol. 41, no. 4, pp. 755–767, Aug. 2004.

[20] R. H. MacArthur and H. S. Horn, "Foliage profile by vertical measurements," *Ecology*, vol. 50, no. 5, pp. 802–804, 1969.

[21] J. D. Aber, "Foliage-height profiles and succession in Northern hardwood forests," *Ecology*, vol. 60, no. 1, pp. 18–23, 1979.

[22] P. J. Besl and N. D. McKay, "A method for registration of 3-D shapes," *IEEE Trans. Pattern Anal. Mach. Intell.*, vol. 14, no. 2, pp. 239–256, Feb. 1992.

[23] R. Bonhomme, C. V. Grancher, and P. Chartier, "Use of hemispherical photographs for determining leaf area index of young crops," *Photosynthetica*, vol. 8, no. 3, pp. 299–301, 1974.

[24] S. G. Leblanc and J. M. Chen, "A practical scheme for correcting multiple scattering effects on optical LAI measurements," *Agric. For. Meteorol.*, vol. 110, no. 2, pp. 125–139, Dec. 2001.

[25] H. Sinoquet and P. Rivet, "Measurement and visualization of the architecture of an adult tree based on a three-dimensional digitising device," *Trees*, vol. 11, no. 5, pp. 265–270, 1997.


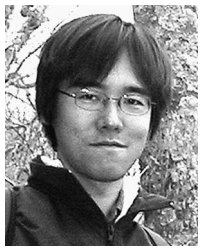

**Fumiki Hosoi** received the M.E. degree from University of Tokyo, Tokyo, Japan, in 1995, where he has been working toward the Ph.D. degree in the Department of Agricultural and Life Sciences since 2005.

In 1995, he joined Opto-Technology Laboratory, Furukawa Electric Company, Ltd., Ichihara, Chiba, Japan.

**Kenji Omasa** received the M.E. degree from Ehime University, Ehime, Japan, in 1975 and the Ph.D. degree in engineering from the University of Tokyo, Tokyo, Japan.

He is currently a Professor with the Department of Agricultural and Life Sciences, University of Tokyo. His research interests include imaging of cell level to plants, remote sensing, modeling of ecosystems, analysis of global change effects on ecosystems and information engineering for biological and environmental systems.